arXiv:cond-mat/9912178v1 [cond-mat.str-el] 10 Dec 1999

Segregation and charge-density-wave order in the spinless Falicov-Kimball model

J. K. Freericks[†] and R. Lemański[*]
[†]*Department of Physics, Georgetown University, Washington, DC 20057 USA*
[*]*Institute of Low Temperatures and Structure Research, Polish Academy of Sciences, Wrocław, Poland*

Abstract

The spinless Falicov-Kimball model is solved exactly in the limit of infinite-dimensions on both the hypercubic and Bethe lattices. The competition between segregation, which is present for large U, and charge-density-wave order, which is prevalent at moderate U, is examined in detail. We find a rich phase diagram which displays both of these phases. The model also shows nonanalytic behavior in the charge-density-wave transition temperature when U is large enough to generate a correlation-induced gap in the single-particle density of states.

Principle PACS number 71.20.Cf. Secondary PACS numbers 71.30.+h and 71.28.+d

Typeset using REVTEX

I. INTRODUCTION

The Falicov-Kimball model[1] is the simplest Fermionic model for crystallization[2], where the system has a phase transition from a disordered (liquid) phase at high temperature to an ordered (solid) phase as the temperature is lowered. It similarly can be viewed as a binary alloy problem where the presence of an ion indicates an A species and the absence of an ion is a B species.

In this model itinerant (spinless) electrons interact with static ions through an on-site Coulomb interaction. Many-body effects enter via the statistical mechanics associated with annealed averaging. It is the simplest many-body problem that can be solved exactly in the limit of large dimensions[3].

Brandt and Mielsch[4] presented the first solution of this problem using dynamical mean-field theory. Their solution illustrated how a period-two charge-density-wave phase is stabilized at low temperatures. Freericks[5] later showed that the model also illustrated incommensurate charge-density-wave order and phase separation. That work concentrated on the case where the ions were half filled on a hypercubic lattice. Segregation was favored at large interaction strength, and incommensurate order disappeared when the interaction strength became larger than the order of the hopping matrix element.

Recent work[6,7] has shown that the segregation principle[8] holds in the infinite-dimensional limit—as T is lowered the system undergoes a phase transition that separates it into electron-rich and ion-rich regions (when the interaction energy becomes infinite). This result, coupled with the rigorous proof of segregation in one-dimension[9] and approximate results in two-dimensions[10,11], provides compelling evidence for segregation to hold in all dimensions. We offer no proof of that statement here. Instead, we just want to comment that such a result is in the same spirit as the Brandt-Schmidt[12] and Lieb-Kennedy[2] result that when the electron and ion concentrations are equal to one-half, the system orders in a period-two ordered phase for all dimensions (and has a finite-temperature phase transition for $d \geq 2$). This tendency toward phase separation could be the mechanism that drives strongly correlated systems like the cuprates or the nickelates towards charge-stripe formation, where the stripes arise from a minimization of the free energy when both the tendency toward phase separation and the long-range Coulomb interaction are taken into account[13]. Further results about the Falicov-Kimball model can be found in a recently completed review[14].

In this contribution we examine what happens to the spinless Falicov-Kimball model as the interaction strength is made finite and the system engages in a competition between phase separation (segregation) and charge-density-wave order. We find a number of interesting results for the phase diagrams that differ from what occurred in the infinite-interaction-strength limit[7].

This manuscript is organized as follows: Section II describes the formalism, Section III presents the results for both the Bethe lattice and the hypercubic lattice, and Section IV presents our conclusions.

II. FORMALISM

The spinless Falicov-Kimball model is represented by the following Hamiltonian:

$$H = -\frac{t^*}{2\sqrt{d}} \sum_{<i,j>} c_i^\dagger c_j + E \sum_i w_i + U \sum_i c_i^\dagger c_i w_i, \tag{1}$$

where $c_i^\dagger$ (c_i) creates (destroys) a conduction electron at lattice site i and $w_i = 0$ or 1 is a classical variable that measures the number of ions at lattice site i. The hopping matrix connects nearest neighbors i and j and has magnitude $t^*/(2\sqrt{d})$ which scales inversely as the square root of the dimensionality d. We choose $t^* = 1$ to be our energy scale. E is the site energy for the ions and U is the on-site Coulomb interaction between electrons and ions. For simplicity we will consider the case of positive U, since negative U can be mapped onto this case with a particle-hole transformation[2].

In the thermodynamic limit, the local lattice Green's function is defined to be

$$G_n = G(i\omega_n) = -\int_0^\beta d\tau e^{i\omega_n \tau} \frac{\mathrm{Tr}\langle e^{-\beta(H-\mu N)} T_\tau c(\tau) c^\dagger(0)\rangle}{\mathrm{Tr}\langle e^{-\beta(H-\mu N)}\rangle}, \tag{2}$$

where $i\omega_n = i\pi T(2n+1)$ is the Fermionic Matsubara frequency, $\beta = 1/T$ is the inverse temperature, N is a number of conduction electrons, and T_τ denotes τ-ordering. A chemical potential μ is used to set the electron concentration $\rho_e = \langle c^\dagger c\rangle$ and the site energy E is adjusted to yield the ion concentration $\rho_i = \langle w\rangle$. The angle brackets in Eq. (2) denote the sum over ionic configurations. The local Green's function is determined by mapping onto an atomic problem in a time-dependent field, with the following action

$$S_{at} = \int_0^\beta d\tau \int_0^\beta d\tau' c^\dagger(\tau) G_0^{-1}(\tau - \tau') c(\tau') + U \int_0^\beta d\tau c^\dagger(\tau) c(\tau) w + Ew, \tag{3}$$

where $w = 0, 1$ is the ion number for the atomic site and G_0^{-1} is the mean-field or effective-medium Green's function, which is determined self-consistently (as described below). The atomic Green's function, with the action in Eq. (3), is computed to be

$$G_n = \frac{1-\rho_i}{G_0^{-1}(i\omega_n)} + \frac{\rho_i}{G_0^{-1}(i\omega_n) - U}, \tag{4}$$

and the local lattice Green's function satisfies

$$G_n = \int_{-\infty}^{\infty} d\epsilon \frac{\rho(\epsilon)}{i\omega_n + \mu - \Sigma_n - \epsilon}, \tag{5}$$

where $\rho(\epsilon)$ is the noninteracting density of states for the infinite lattice and Σ_n is the self-energy. The self-consistency relation is that the self-energy Σ_n in Eq. (5) must coincide with the self-energy of the atomic problem, i. e.

$$\Sigma(i\omega_n) = G_0^{-1}(i\omega_n) - G_n^{-1}. \tag{6}$$

Equations (4), (5), and (6) constitute the dynamical mean-field theory for homogeneous phases. In the limit $d \to \infty$ Eq. (6) is an exact equation for the lattice problem.

These equations must be solved numerically for the general case (an analytic simplification[7] occurs on the Bethe lattice when $U = \infty$). We use Jarrell's iterative algorithm[15] to solve this problem: (i) begin with the self-energy set equal to zero $\Sigma_n = 0$; (ii) use Eq. (5) to determine the local Green's function; (iii) solve for the effective medium by

employing Eq. (6); (iv) find the new local Green's function from Eq. (4); (v) extract a new self energy from Eq. (6); and (vi) repeat steps (ii-v) until the self-energy does not change from one iteration to the next. We use a relative error of one part in 10^7 as our convergence criterion. These equations rapidly converge in most cases, but occasionally require damping of oscillations to force them to converge, rather than enter a periodic limit cycle. These equations can also be solved on the real axis, where the Matsubara frequency is replaced by the real frequency ($i\omega_n \rightarrow \omega + i\delta$).

At high temperatures the system is in a homogeneous phase, with a uniform charge density. As T is lowered, the system can undergo a phase transition to a charge density wave. The temperature below which the homogenous phase is unstable is found by calculating the divergence of the relevant susceptibility. The detailed formulas for these susceptibilities have appeared elsewhere[4,5,16] and will not be repeated here. We do not consider incommensurate order in this contribution. Incommensurate order is easily handled in the hypercubic lattice[4,5], but is problematic on the Bethe lattice, where it appears that higher-order periodic phases always have first-order phase transitions[17]. We investigate two different possibilities here: (i) the two-sublattice chessboard charge-density-wave phase, which has different electron and ion charge densities on the two sublattices of the bipartite lattice, and (ii) the segregated phase, where the system separates into two uniform phases with different electron and ion densities. The former is the $(\pi, \pi, \pi, ...)$ susceptibility and the latter is the uniform susceptibility.

We also need to calculate the Helmholz free energy for these systems in order to perform a Maxwell construction to track the first-order phase transition to the segregated phase (the transition to the chessboard phase is always continous). This free energy can be expressed either as a summation over Matsubara frequencies, as first shown by Brandt and Mielsch[4], or it can be expressed as an integral over the interacting density of states, as first shown by Ramirez, Falicov, and Kimball[1]. We choose the former form, since there is no analytic form for the interacting density of states when U is finite. Hence, the free energy becomes

$$F(\rho_e, \rho_i) = -T \ln 2 + T\rho_i \ln \rho_i + T(1-\rho_i)\ln(1-\rho_i) + \mu(\rho_e - \frac{1}{2}) + \frac{U\rho_i}{2} \tag{7}$$
$$+T \int d\epsilon \rho(\epsilon) \sum_n \ln[\frac{G_0(i\omega_n) i\omega_n}{(i\omega_n + \mu - \Sigma_n - \epsilon)G_n}] - T\rho_i \sum_n \ln[1 - UG_0(i\omega_n)].$$

One must be careful in evaluating this expression, since the integrand, which involves the summation of a logarithm over the Matsubara frequencies, requires a large frequency cutoff to converge.

The Maxwell construction for the phase-separated (segregated) state consists of taking a weighted average of the free energy in two homogeneous phases with densities $(\rho_e^{(1)}, \rho_i^{(1)})$ and $(\rho_e^{(2)}, \rho_i^{(2)})$ subject to the system having the correct *average* electron and ion concentration. In equations, we take

$$F_{seg}(\rho_e, \rho_i) = \alpha F(\rho_e^{(1)}, \rho_i^{(1)}) + (1-\alpha) F(\rho_e^{(2)}, \rho_i^{(2)}) \tag{8}$$

where

$$\rho_e = \alpha \rho_e^{(1)} + (1-\alpha)\rho_e^{(2)}, \tag{9}$$

$$\rho_i = \alpha\rho_i^{(1)} + (1-\alpha)\rho_i^{(2)} \tag{10}$$

The electron concentrations are determined by setting a common chemical potential between the two phases and the constraint of Eq. (9). Of the six parameters (α, μ, $\rho_e^{(1)}$, $\rho_e^{(2)}$, $\rho_i^{(1)}$, and $\rho_i^{(2)}$) needed to specify the segregated phase, only two are independent variables. We use the ion concentrations $\rho_i^{(1)}$ and $\rho_i^{(2)}$ as our independent variables. Our minimization procedure is identical to the one used in the infinite-U case[7]: (i) we first choose a coarse grid for both $\rho_i^{(1)}$ and $\rho_i^{(2)}$ and compute the average free energy for all points on that grid, and locate the minimum; (ii) the ion density $\rho_i^{(1)}$ is fixed at this coarse minimum, and $\rho_i^{(2)}$ is varied over a fine grid to find the new minimum; (iii) the ion density $\rho_i^{(2)}$ is fixed at this new minimum, and $\rho_i^{(1)}$ is varied over a fine grid to find the new minimum; and (iv) both ion densities are varied over a final fine grid centered at the approximate minimum to complete the minimization procedure. We find that the minima rarely change in step (iv) which illustrates the convergence of this method. This multistep convergence procedure is much more efficient than just minimizing over the fine grid from the start.

III. RESULTS

We perform calculations for two different lattices—the infinite-coordination-number Bethe lattice where $\rho(\epsilon) = \sqrt{4-\epsilon^2}/(2\pi)$ and the infinite-dimensional hypercubic lattice where $\rho(\epsilon) = \exp(-\epsilon^2)/\sqrt{\pi}$. In general, computations for the Bethe lattice are simpler than for the hypercubic lattice, because many of the integrals over the density of states can be performed analytically. But we find that there is little difference between the results for the two lattices, as can be seen in the results presented below.

We begin by showing the transition temperatures to the chessboard (two-sublattice) charge density wave and the spinodal-decomposition temperature for segregation, as determined by finding the temperature where the relevant susceptibility diverges. Figure 1 displays the results for the case where $\rho_i = 0.2$ on the Bethe lattice for two different values of U. In the weak-coupling regime, there is no competition between the chessboard phase and segregation, because the two regions do not overlap, but when U is made larger, one can see an overlap between these regions. It may appear then that there are regions in the weak-coupling regime where the homogenous phase is stable all the way down to $T = 0$, but we believe that this will not be the case in general. As seen in the work on the hypercubic lattice at $\rho_i = 0.5$, the region that appeared to be a homogeneous phase turned out to be one that displayed incommensurate order[5]. We expect a similar result to take place here, but due to the difficulty in calculating incommensurate order on the Bethe lattice (which is typically a first-order transition) we have not investigated that question here.

Furthermore, a kink appears in the $T_c(\rho_e)$ curve for the chessboard phase. This kink occurs at the filling $\rho_e = 1 - \rho_i$, which is a special filling for the spinless Falicov-Kimball model. When U is large enough, this is the filling where the system undergoes a metal-insulator transition (in this case with $\rho_i = 0.2$ the critical value of U is approximately 1.86). The interacting density of states for the electrons generates a gap, and increasing the electron filling from just below $1 - \rho_i$ to just above $1 - \rho_i$ results in a large shift in the electronic chemical potential as it moves from the lower to the upper band[18]. What is remarkable is that

this metal-insulator transition illustrates itself via a kink in the chessboard phase transition temperature! A similar result can be seen in the Hubbard model, but was not pointed out in the original paper[19]. Beyond $U = 3$ the antiferromagnetic transition temperature curves display the same kink at half filling as seen in the Falicov-Kimball model, and the presence of such kinks appears to be another way to infer that the system has a gap in the single-particle density of states, which does not require performing calculations on the real axis (which are much more difficult for quantum Monte Carlo simulations).

In Figure 2 we show the spinodal-decomposition temperature for segregation on the Bethe lattice for both $\rho_i = 0.5$ and $\rho_i = 0.2$. Notice how the two pieces of the phase diagram move towards each other to meet at $\rho_e = 1-\rho_i$. We also include the result for $U = \infty$ which has a mirror symmetry about the line $\rho_e = (1-\rho_i)/2$. That symmetry is absent for finite-U and develops slowly as U increases. There are no states at finite energy with $\rho_e > 1-\rho_i$ when $U = \infty$ so only one branch is included in the spinodal-decomposition temperature.

The transition temperature to the chessboard phase on the Bethe lattice is shown in Figure 3 for the same cases $\rho_i = 0.5$ and $\rho_i = 0.2$. Here we separate the figures into those at weak coupling (a) and (c), where there is no kink in the phase diagram, and those at strong coupling (b) and (d), where a kink is present because of the gap in the single-particle density of states (for $\rho_i = 0.5$ this occurs at $U = 2$). The chessboard phase is stable only in a narrow window around $\rho_e = 1 - \rho_i$ when U is large, but migrates towards $\rho_e = 0.5$ for smaller values of U. The competition between segregation and the chessboard phase is the strongest when $\rho_e \approx 1-\rho_i$ and U is around two times of the bandwidth. Notice how the case with $\rho_i = 0.5$ displays an additional reflection symmetry about $\rho_e = 0.5$. This particle-hole symmetry disappears, and the phase diagrams possess a strong asymmetry when $\rho_i \neq 0.5$.

Figures 4 and 5 display the identical results as Figures 2 and 3 respectively, but this time are plotted for the hypercubic lattice rather than the Bethe lattice. It is remarkable how similar the results are for these two lattices (with the exception of an overall scale factor). The kinks in the chessboard phase diagram appear to be sharper on the hypercubic lattice, but otherwise the results are nearly identical with each other. Due to the similarity of the results for the Bethe and hypercubic lattices, we have chosen to concentrate only on the computationally simpler Bethe lattice for the free-energy analysis (we have verified the similarity of the free-energy phase diagrams for the hypercubic and Bethe lattices for a few cases).

A Maxwell construction is needed to calculate the phase diagram when the system phase separates. Just like the case where $U = \infty$, we find that the phase diagram has special homogeneous densities (ρ_e^*, ρ_i^*) where the first-order phase transition (binodal, T_b) and the spinodal-decomposition temperature (spinodal, T_s) coincide. The point corresponds to a critical temperature $T_c = T_{s,\,\max}$) where for a given U both the first-order transition temperature and the spinodal-decomposition temperature share a maximum. At this point both of the electron densities approach the homogeneous density ($\rho_e^{(1)} \to \rho_e^*$ and $\rho_e^{(2)} \to \rho_e^*$) as the temperature approaches the transition temperature from below (and likewise for ρ_i). Obviously the transition is continuous at this point. In the general case, we find only one of the two pairs tends towards the homogeneous values of the fillings as T_b is approached, and the phase transition is discontinuous (in this case we find α approaches either 0 or 1 as T_b is approached). The phase diagrams are complicated three-dimensional curves in ρ_i, ρ_e, and T space. We project those curves onto different planes in order to summarize our results.

Figure 6 contains the projection of the segregation phase diagram onto the ρ_e–ρ_i plane for the Bethe lattice. The diamonds indicate the values of the electron and ion concentrations at the maximum of the spinodal-decomposition temperature for a given value of U. These maxima are monotonic in ρ_e, but are nonmonotonic in ρ_i increasing from 0.58 at $U = 0.25$ to 0.8 for $U = 2$ and then decreasing to 0.65 as $U \to \infty$. The solid curves display the pairs of densities that the system phase separates into as a function of temperature when in the segregated phase. As $T \to 0$ we find all systems go to the states with $\rho_e^{(1)} = 0$ and $\rho_i^{(1)} = 1$ and $\rho_e^{(2)} = \rho_e^*/(1-\rho_i^*)$ and $\rho_i^{(2)} = 0$. The dashed lines are straight lines that connect these two points, and are guides to the eye. The chain-dashed line is a similar plot for the case where $U = \infty$. Note how these solid curves are nearly straight lines for both small and large U, and how they become curved only for cases of intermediate U. The maximal spinodal-decomposition temperature does monotonically increase with U as shown in Figure 7.

It is remarkable that the results we obtained in the infinite-dimension limit as $T \to 0$ are similar to those found in the ground-state in one dimension[20–22] and two dimensions[10,11]. In all these cases (for $U > 0$) the segregated phase characterized by the pair of densities (ρ_e, ρ_i) is a mixture of the fully occupied phase (where the ions clump together) without electrons, i.e. $(\rho_e^{(1)}, \rho_i^{(1)}) = (0, 1)$ and the empty phase (without ions) with a finite density of electrons equal to $\rho_e/(1-\rho_i)$, i.e. $(\rho_e^{(2)}, \rho_i^{(2)}) = (\rho_e/(1-\rho_i), 0)$. The two regions where the segregated phase is stable consist of those points of the (ρ_e, ρ_i) plane that satisfy one of the inequalities: $0 < \rho_e < (1-\rho_i)b_d(U)$ or $(1-\rho_i)b_d(U) < \rho_e < 1$, where $b_d(U)$ $[b_d(U) > 0]$ is an increasing function of U tending towards unity when U goes to infinity (d denotes the spatial dimension). In the one-dimensional case a transcendental equation for $b_1(U)$ has been derived[21].

With an increase of U, the stability of the segregated phase for the one and two-dimensional phase diagrams spreads over the whole region of densities ρ_e and ρ_i except for the unit-density case $\rho_e + \rho_i = 1$, where periodic phases are stable. In one dimension, the unit-density phase corresponds to the most homogenous distribution of the ions for any U. In two dimensions, the ions are also arranged periodically (in the unit-density case) but their arrangement changes with U (there is no unique "most homogenous distribution" in two dimensions).

If $\rho_i = 0.5$ and the unit-density condition is fulfilled ($\rho_i + \rho_e = 1$), then the charge-ordered phase is found to be stable in the infinite-dimensional limit (in fact, this is also for a region of ρ_e close to that given by the unit-density condition). However our calculations show this property is relevant for moderate U only. Presumably the order of the limits $d \to \infty$; $U \to \infty$ and $\rho_e \to 1 - \rho_i$ must be taken properly to get the charge-density order in this case. We cannot compare the one and two-dimensional results for $\rho_i = 0.2$ ($\rho_e = 1 - \rho_i = 0.8$) with those in the infinite U limit because we rectricted ourselves (for technical reasons) to the chessboard-type charge-ordering only.

For finite U, the rest of the (ρ_e, ρ_i) region (apart from the areas occupied by the segregated and the unit-density phases) of the one and two-dimensional phase diagrams contain a number of charge-density-wave phases that differ from the chessboard one (as well as their mixtures). We expect that the similar effect will occur in the infinite-dimensional limit for intermediate densities, where the homogenous phase appeared to be stable down to zero temperature (see Fig. 1), but where we expect incommensurate order to prevail.

Figures 8 and 9 show the projection of the phase diagram onto the ρ_e–T and ρ_i–T planes respectively. At any given temperature, a horizontal line intersects a solid line of the phase diagram at two points, corresponding to the pair $(\rho_e^{(1)}, \rho_e^{(2)})$ and $(\rho_i^{(1)}, \rho_i^{(2)})$ respectively. The solid lines are the binodal (first-order) phase-transition lines, and the dashed lines are the spinodal (second-order) phase-transition lines where the system becomes locally unstable. Although these phase diagrams appear to have similar shapes to those seen at $U = \infty$, we were unable to determine any kind of appropriate scaling form which could collapse the data onto an universal scaling form.

An example of the general case, where the phase transition is discontinuous, is shown in Figure 10. Here the spinodal and binodal transition temperatures are not equal to each other for a given pair of densities (ρ_e, ρ_i). We have chosen the case of $\rho_e = 0.15$, $\rho_i = 0.5$, and $U = 4$, and show results only for the ρ_i–T plane. Note that one of the ion densities has a discontinous jump at T_b whereas the other one changes smoothly when the temperature is lowered below T_b. This occurs because of the nucleation of the new phase inside the (old) high-temperature phase.

IV. CONCLUSIONS

The main result of this work is the pervasiveness of phase separation and the segregation principle in the Falicov-Kimball model in infinite-dimensions. We see that it survives for all values of U, and that it can take up a large portion of the phase space in the system. In addition, the transition temperatures become larger as U grows, and the phase-separated state takes over the entire phase diagram except possibly the point where $\rho_e = 1 - \rho_i$. Since this is precisely the result seen in the one-dimensional[9] and two-dimensional[10,11] cases, this result strongly suggests that the phenomenon of segregation is indeed independent of dimensionality. Such a general principle should have a fundamental physical reason that drives its behavior, and this begs for a general proof that would hold in arbitrary dimensions. We offer no such proof here, since we are unable to determine what this general principle is. In one dimension, segregation is driven by a lowering of the kinetic energy by placing all electrons in as large a "box" as possible. This kinetic-energy-driven effect should hold in all dimensions, but the analysis is much more complicated for $d > 1$. We do believe that this general principle is important in the phenomena of stripes, since it must contribute to the ability of a system like the Hubbard model to form stripes.

We also find that there are some regions where this segregation can compete with charge-density-wave order. These regions are fairly small in the phase diagram, since they occur near $\rho_e = 1 - \rho_i$ for moderate values of U. In this region there can also be competition between incommensurate order (which we have not considered due to it's technical difficulties on the Bethe lattice) and either phase separation or chessboard charge-density-wave order.

Finally, we discovered an interesting slope discontinuity (nonanalyticity) in the chessboard-phase transition temperature which occurs when the single-particle density of states generates a correlation-induced gap. Such a signature of a correlation-induced gap is ubiquitous, and it can also be seen in the Hubbard model when it is beyond the Mott transition. While we believe the formation of an anomalous kink in the phase diagram implies the generation of a correlation-induced gap, we once again offer no proof, and simply

state that such an observation will shed insight on metal-insulator transitions, but it is not a substitute for calculations of the single-particle density of states.

REFERENCES

[1] L. M. Falicov and J. C. Kimball, Phys. Rev. Lett. **22**, 997 (1969); R. Ramirez, L. M. Falicov, and J. C. Kimball, Phys. Rev. B **2**, 3383 (1970).
[2] T. Kennedy and E. H. Lieb, Physica A **138**, 320 (1986).
[3] W. Metzner and D. Vollhardt, Phys. Rev. Lett. **62**, 324 (1989).
[4] U. Brandt and C. Mielsch, Z. Phys. B **75**, 365 (1989); **79**, 295 (1990); **82**, 37 (1991).
[5] J. K. Freericks, Phys. Rev. B **47**, 9263 (1993).
[6] B. M. Letfulov, Eur. Phys. J. B **4**, 447 (1998); **11**, 423 (1999).
[7] J. K. Freericks, Ch. Gruber, and N. Macris, Phys. Rev. B **60**, 1617 (1999).
[8] J. K. Freericks and L. M. Falicov, Phys. Rev. B **41**, 2163 (1990).
[9] P. Lemberger, J. Phys. A **25**, 715 (1992).
[10] C. Gruber, J. Jędrzejewski and P. Lemberger, J. Stat. Phys. **66**, 913 (1992).
[11] G. I. Watson and R. Lemański, J. Phys.: Condens. Matter **7**, 9521 (1995).
[12] U. Brandt and R. Schmidt, Z. Phys. B **63**, 45 (1986).
[13] O. Zahar, S. A. Kivelson, and V. J. Emery, Phys. Rev. B **57**, 1422 (1998).
[14] Ch. Gruber and N. Macris, Helv. Phys. Acta **69**, 850 (1996).
[15] M. Jarrell, Phys. Rev. Lett. **69**, 168 (1992).
[16] J. K. Freericks and V. Zlatić, Phys. Rev. B **58**, 322 (1998).
[17] Ch. Gruber, N. Macris, Ph. Roger, and J. K. Freericks, unpublished.
[18] P. G. J. van Dongen and C. Leinung, Ann. Physik **6**, 45 (1997).
[19] J. K. Freericks and M. Jarrell, Phys. Rev. Lett. **74**, 186 (1995).
[20] J. Lach, R. Łyżwa and J. Jędrzejewski, Phys. Rev B **48**, 10783 (1993).
[21] C. Gruber, D. Ueltschi and J. Jędrzejewski, J. Stat. Phys. **76**, 125 (1994).
[22] Z. Gajek, J. Jędrzejewski and R. Lemański, Physica A **223**, 175 (1996).

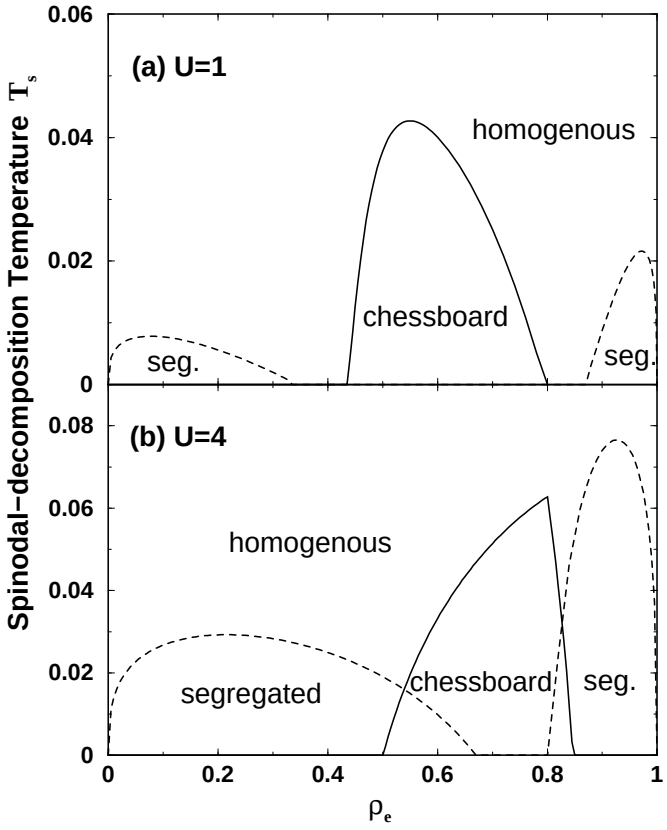

FIG. 1. Phase diagrams to the chessboard charge-density-wave phase and the spinodal-decomposition temperature for the segregated phase on the Bethe lattice with $\rho_i = 0.2$. Figure 1(a) is the case $U = 1$ where the chessboard phase and the segregated phase do not compete with each other. Figure 1(b) is the case with $U = 4$ where there is an overlap of the spinodal phase lines, indicating a competition between segregation and charge density wave formation, and where a well-developed kink can be seen in the chessboard phase diagram, which occurs due to a correlation-induced gap in the single-particle density of states, as described in the text.

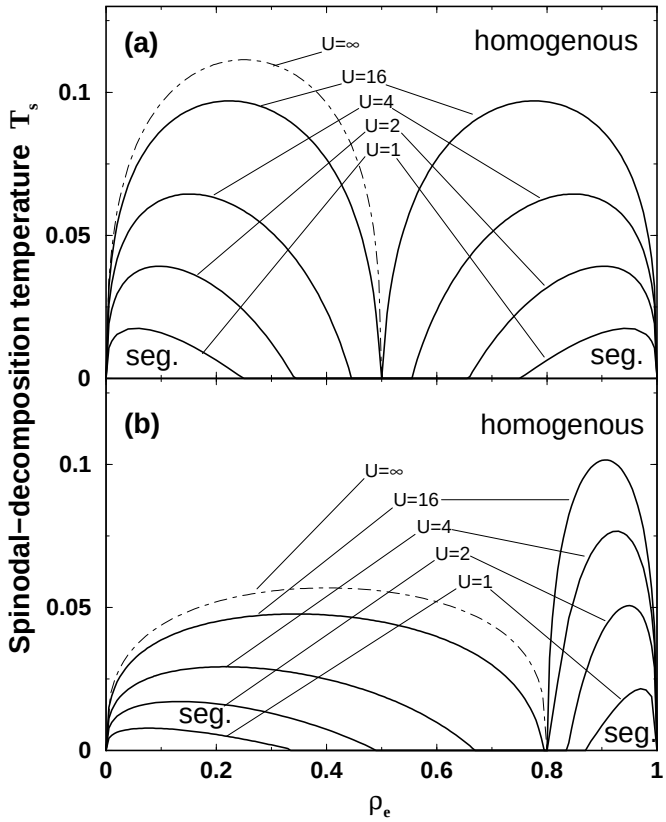

Figure 2, Phys. Rev. B, Freericks and Lemanski

FIG. 2. Spinodal decomposition temperature for the segregated phase on the Bethe lattice as a function of U: (a) the case $\rho_i = 0.5$ and (b) the case $\rho_i = 0.2$. The chain-dashed line corresponds to $U = \infty$ where only the lower branch is relevant.

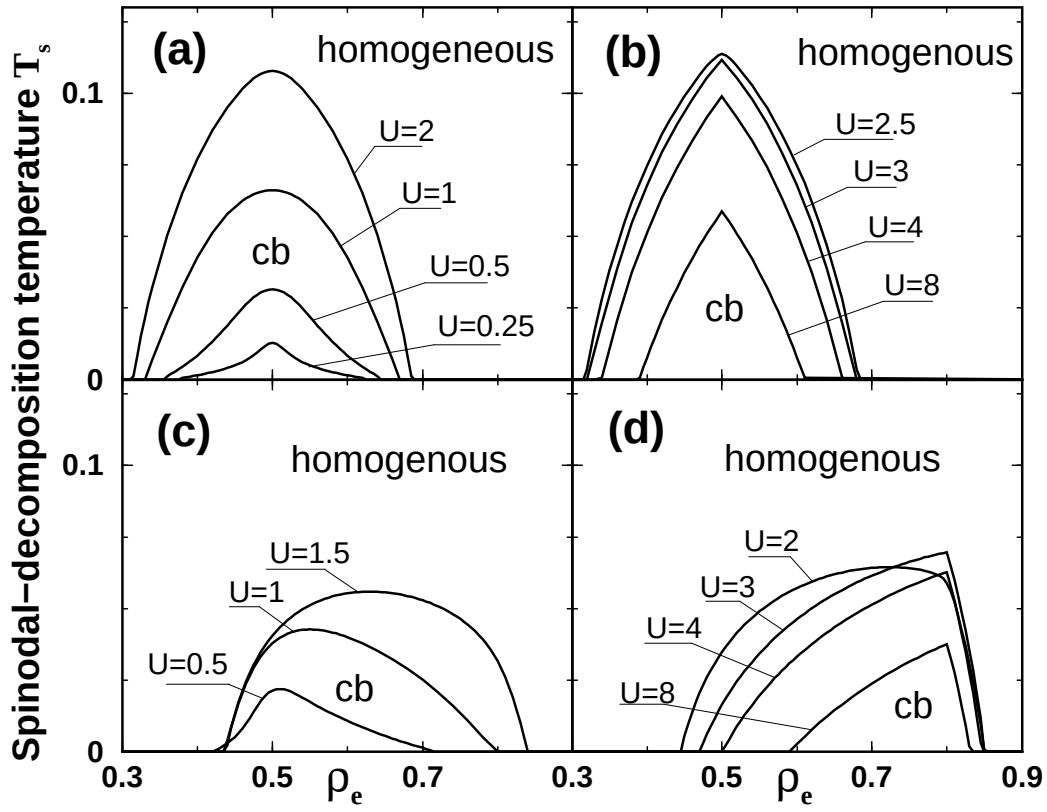

Figure 3, Freericks and Lemanski, Phys Rev. B

FIG. 3. Phase diagram for the chessboard (cb) charge-density-wave phase on the Bethe lattice: (a) $\rho_i = 0.5$ and small U, where the curve is smooth; (b) $\rho_i = 0.5$ and large U, where the curve develops a kink at $\rho_e = 0.5$; (c) $\rho_i = 0.2$ and small U, where the curve is smooth; and (d) $\rho_i = 0.2$ and large U, where the curve develops a kink at $\rho_e = 0.8$.

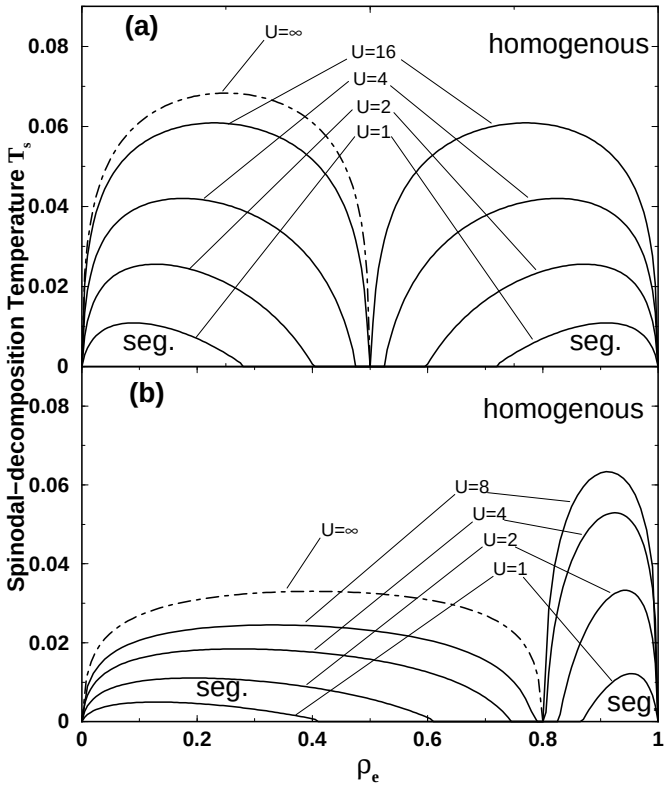

Figure 4, Phys. Rev. B, Freericks and Lemanski

FIG. 4. Spinodal decomposition temperature for the hypercubic lattice as a function of U: (a) the case $\rho_i = 0.5$ and (b) the case $\rho_i = 0.2$. The chain-dashed line corresponds to $U = \infty$ where only the lower branch is relevant. Note the similarity with Figure 2.

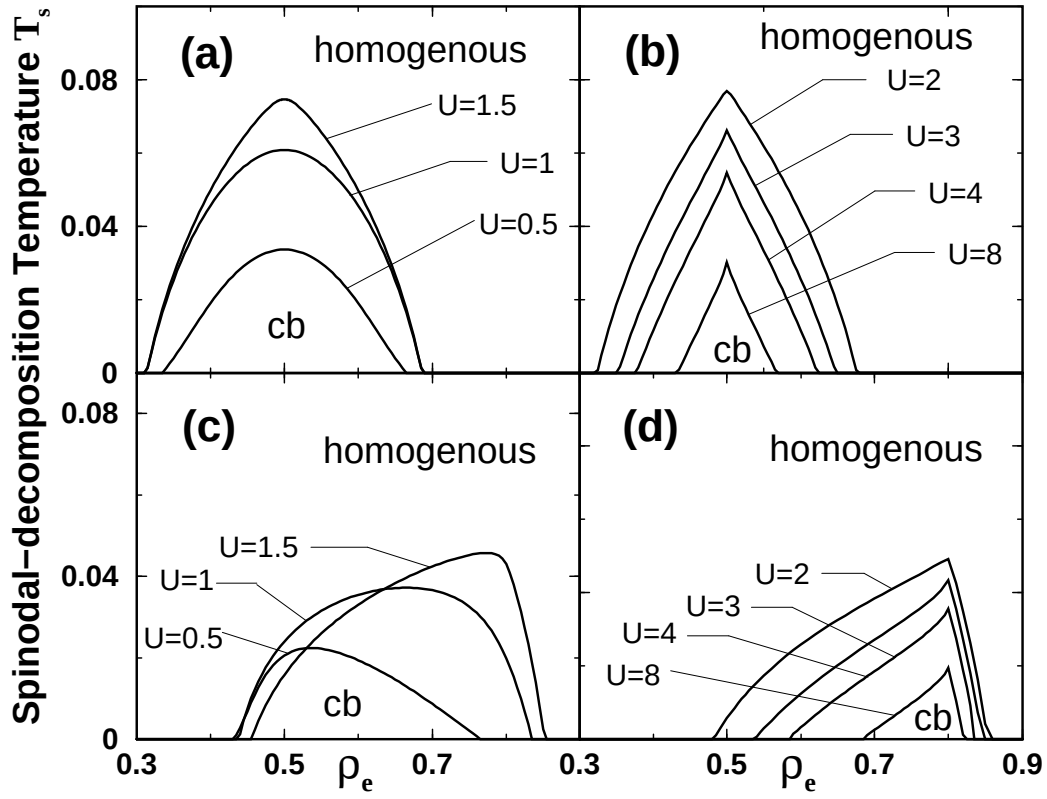

Figure 5, Phys. Rev. B, Freericks and Lemanski

FIG. 5. Phase diagram for the chessboard charge-density-wave phase on the hypercubic lattice: (a) $\rho_i = 0.5$ and small U, where the curve is smooth; (b) $\rho_i = 0.5$ and large U, where the curve develops a kink at $\rho_e = 0.5$; (c) $\rho_i = 0.2$ and small U, where the curve is smooth; and (d) $\rho_i = 0.2$ and large U, where the curve develops a kink at $\rho_e = 0.8$. Note how the only difference with Figure 3 is that the kinks are more strongly developed here.

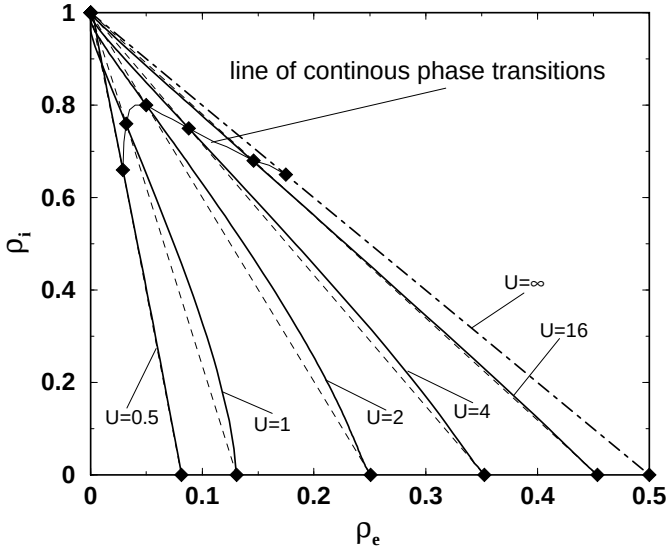

Figure 6, Phys. Rev. B, Freericks and Lemanski

FIG. 6. Projections of the segregation phase diagram onto the ρ_e–ρ_i plane for the Bethe lattice. The solid diamonds connected by the solid curve near $\rho_i = 0.7$ denote the homogeneous densities where the spinodal-decomposition temperature is a maximum for a given value of U. The solid lines are the values of the densities at various temperatures, and the dashed lines are straight-line guides to the eye. The chain-dashed line is the result with $U = \infty$.

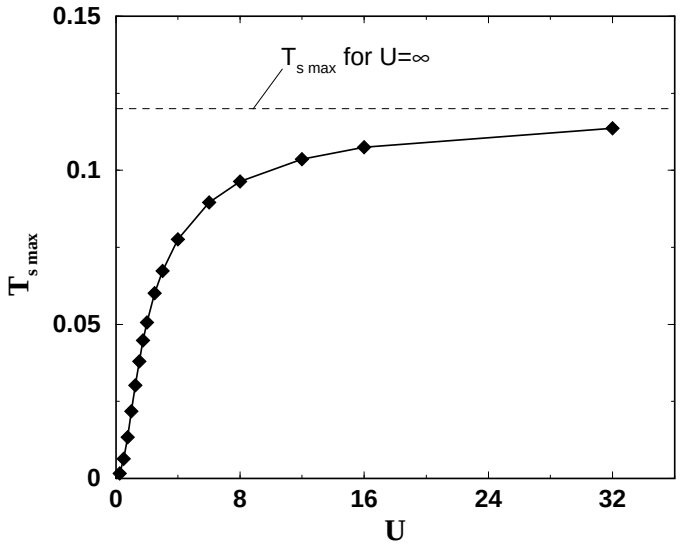

Figure 7, Phys. Rev. B, Freericks and Lemanski

FIG. 7. Maximal spinodal-decomposition temperature on the Bethe lattice plotted as a function of U.

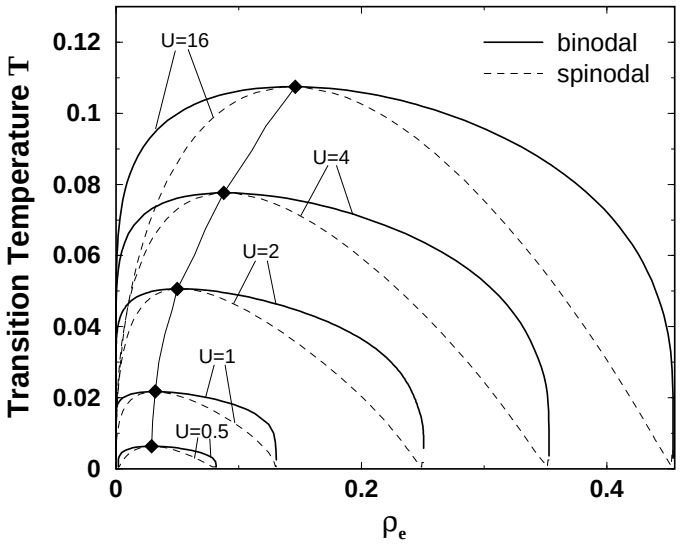

Figure 8, Phys. Rev. B, Freericks and Lemanski

FIG. 8. Projection of the segregation phase diagram onto the ρ_e–T plane for the Bethe lattice. The diamonds denote the homogeneous densities where the spinodal-decomposition temperature is a maximum for a given value of U (which corresponds to the classical critical point). The solid lines are the binodal (first-order) transition temperatures, and the dashed lines are the spinodal-decomposition temperatures.

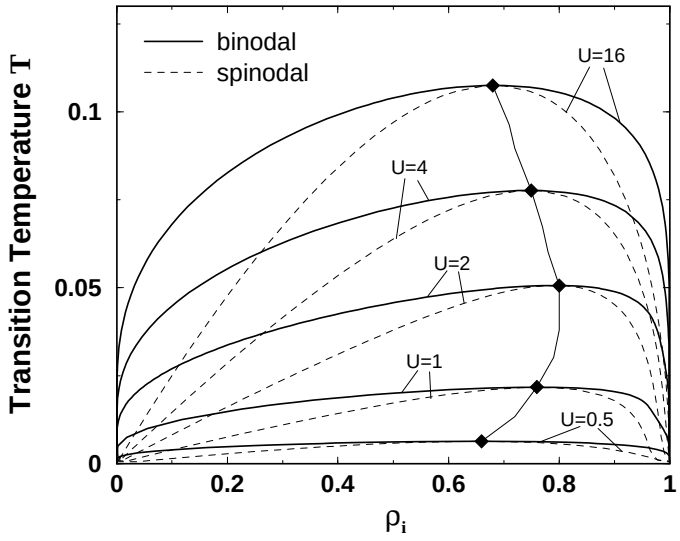

Figure 9, Phys. Rev. B, Freericks and Lemanski

FIG. 9. Projection of the segregation phase diagram onto the ρ_i–T plane for the Bethe lattice. The diamonds denote the homogeneous densities where the spinodal-decomposition temperature is a maximum for a given value of U. The solid lines are the binodal (first-order) transition temperatures, and the dashed lines are the spinodal-decomposition temperatures. Note how the maximal ion density is not monotonic in U.

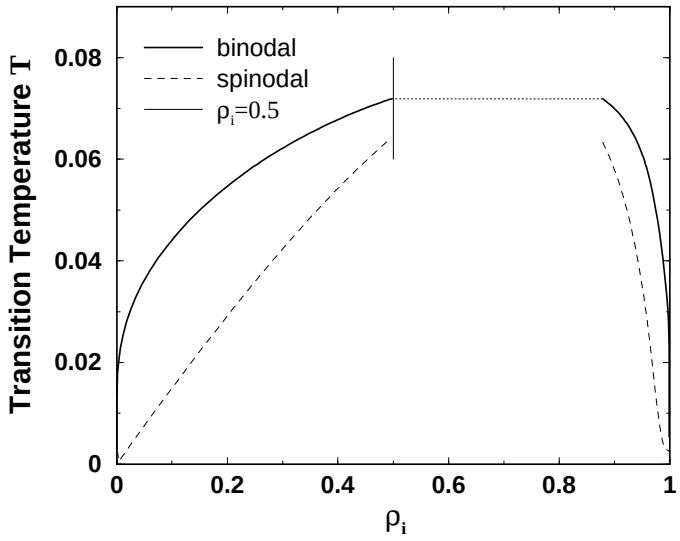

Figure 10, Phys. Rev. B, Freericks and Lemanski

FIG. 10. Projection of the segregation phase diagram onto the ρ_i–T plane for the Bethe lattice in a generic discontinuous case ($\rho_e = 0.15$ and $\rho_i = 0.5$). The solid line is the binodal (first-order) transition temperature, and the dashed line is the spinodal-decomposition temperature. A horizontal line is included at $\rho_i = 0.5$ as a reference.